

Top cross section in the LHeC and FCC-he energy range

G.R.Boroun*

Department of Physics, Razi University, Kermanshah 67149, Iran
(Dated: January 16, 2023)

Predictions of the top-pair production cross section in electron-proton (ep) collisions at the future circular collider hadron-electron (FCC-he) and the large hadron electron collider (LHeC) in the leading order (LO) and the next-to-leading order (NLO) approximations in perturbative quantum chromodynamics (QCD) are presented. Numerical results for the top structure functions and the ratio of structure functions are computed at the renormalization scale $\mu^2 = Q^2 + 4m_t^2$ in the collinear generalized double asymptotic scaling (DAS) approach. These results are presented in terms of the effective parameters of the parameterization of $F_2(x, Q^2)$, where relying on a Froissart-bounded. These quantitative results can be important for future collider experiments at the center-of-mass energy frontier and the improvement of the phenomenological models for the development of the cosmic ray cascades in ultra-high-energy domain. We obtained the uncertainties because of the power-law behavior $x^{-\Delta}$ of the collinear parton distribution functions (PDFs), the factorization, and renormalization scales, on the top properties at high inelasticity for the FCC-he center-of-mass (CM) energy at the NLO approximation.

I. INTRODUCTION

Top physics at future electron-proton colliders will be highlighted to show the future progress in the large hadron electron collider (LHeC) and future circular collider hadron-electron (FCC-he) accelerators [1,2]. The main goal of the future at the LHeC and FCC-he is to achieve a deeper knowledge of the hadronic structure at high energies through the deep inelastic scattering (DIS) process, where an electron emits a virtual photon that interacts with a proton target. In particular, the proton structure can be studied through the γ^*p interaction, with the behavior of the observables being determined by the QCD dynamics at high energies. These ep colliders (i.e., LHeC and FCC-he), with those smaller backgrounds, can be of great importance in illuminating the nature of the new physics for top-pair production. The top quark can be produced by the LHeC and FCC-he colliders in $\gamma^*p \rightarrow t\bar{t}X$ reactions [3]. For the first time, at the LHeC, the top-pair production can be studied in DIS. According to the standard model (SM), top -pair is produced dominantly in gluon-boson fusion at $x < 0.1$. The LHeC opens top quark parton distribution function (PDF) physics as a new field of research. Top -quark production could not be observed at hadron-electron ring accelerator (HERA), but it will become a major topic of precision physics and discovery in the LHeC and FCC-he colliders.

A single top is produced in charged currents (CC), with a total cross section of order 5 pb, which can easily be estimated from the leading -order (LO) calculation of Wb scattering [2] or 1.89 pb as reported in Ref.[1] at a center-

of-mass energy of 1.3 TeV, i.e., with an electron-beam energy of 60 GeV and an LHC proton beam of 7 TeV. In CC, this leads to a top-beauty final state, while in neutral currents (NC) this gives rise to a pair producing top-antitop quarks in photoproduction and DIS. Photoproduction of the top-antitop quark pairs ($\gamma g \rightarrow t\bar{t}$) is the second most important production mode for top quarks at the LHeC as a total cross -section of 0.05 pb is expected at the LHeC. Furthermore, the DIS regime of $t\bar{t}$ production will allow us to probe the top cross section. In DIS, the total cross section for top quark pair production mode is ~ 53 fb at the LHeC and ~ 1 pb at the FCC-he [4]. Here, it may be useful to refer to older discussions about heavy-quark production. The authors in Refs.[5] and [6] studied the top quark production in ep-collisions at HERA energies. In electron -proton colliders like HERA, a heavy quark pair is created via the boson-gluon fusion (BGF) mechanism [5], where the electromagnetic coupling in $ep \rightarrow t\bar{t}X$ pair production is defined by the following interaction lagrangian density

$$\mathcal{L}_{em} = -\sqrt{4\pi\alpha_{EM}} \left[e_e \bar{\Psi}_e \gamma^\mu \Psi_e + e_t \bar{\Psi}_t \gamma^\mu \Psi_t \right] A_\mu. \quad (1)$$

Here, the Dirac fields Ψ_e , Ψ_t and the vector field A_μ describe the electron, the top and the photon, respectively. In Eq.1, e_e and e_t give, respectively, the electric charge of electron and top -quark in units of $\sqrt{4\pi\alpha_{EM}}$, where α_{EM} is the fine structure constant. The cross section in the BGF is given by the formula

$$d\sigma = \frac{1}{8} \frac{1}{4\mathbf{p}\cdot\mathbf{l}} G(z, s) dz dPS^{(3)} \sum_{\text{spins}} |M_t|^2. \quad (2)$$

Here, $G(z, s)$ is the gluon distribution where the momentum scale of the gluon density has been chosen to correspond to the total invariant energy s of the produced

*Electronic address: boroun@razi.ac.ir

top quark system. \mathbf{p} and \mathbf{l} are momentum of gluon and lepton in the subprocess, and $dPS^{(3)}$ is the three-particle phase space. The exact solution of the total cross section is described in Refs.[5] and [6]. A useful approximate form of the exact total cross-section for the large values of \sqrt{s} is provided by the Weizsäcker-Williams (WW) approximation [7], which provides a convenient framework to derive simple approximate forms of Eq.(2), as

$$\sigma = \int_{y_{\min}}^1 dy P_\gamma(y) \int_{z_{\min}}^1 dz G(z, M_p^2) \hat{\sigma}, \quad (3)$$

where P_γ is the photon -splitting function and $\hat{\sigma}$ is the cross section of the $t\bar{t}$ pair production by a real photon and $z_{\min} = (4m_t^2 + Q^2)/(ys)$. The WW approximation agrees with the exact pair production for top quarks as discussed in the literature [5,6]. The corresponding hadron-level cross sections, $\sigma_{k=2,L}^t$ in the fixed-flavor-number scheme (FFNS), has the form [8]

$$\sigma_k^t = \int_{z_{\min}}^1 dz G(z, \mu_F) \hat{\sigma}_{k,g}^t\left(\frac{x}{z}, \mu_F, \mu_R\right), \quad (4)$$

where $G = xf_g$ is the gluon distribution function of the proton. μ_R and μ_F are the renormalization and factorization scales, respectively. Here, $\hat{\sigma}_{k,g}^t$, ($k = 2, L$) are the γ^*g cross sections as at LO approximation, the photon-gluon component of the heavy-quark leptonproduction is described by the following parton-level interaction:

$$\gamma^* + g \rightarrow t + \bar{t}.$$

The leptonproduction cross sections $\sigma_{k=2,L}^t(x, Q^2)$ are related to the structure functions $F_k^t(x, Q^2)$ as follows:

$$\begin{aligned} F_L^t(x, Q^2) &= \frac{Q^2}{8\pi^2\alpha_{EM}x} \sigma_L^t(x, Q^2), \\ F_2^t(x, Q^2) &= \frac{Q^2}{4\pi^2\alpha_{EM}} \sigma_2^t(x, Q^2). \end{aligned} \quad (5)$$

In the case of unpolarized initial states and neglecting the contribution of Z-boson exchange, the structure functions are related to the double differential cross section by the following form:

$$\begin{aligned} \frac{d^2\sigma^{t\bar{t}}}{dx dQ^2} &= \frac{2\pi\alpha_{EM}^2}{xQ^4} \left\{ [(1 + (1 - y)^2)] F_2^t(x, Q^2) \right. \\ &\quad \left. - y^2 F_L^t(x, Q^2) \right\}, \end{aligned} \quad (6)$$

where $y = Q^2/sx$ is the inelasticity with s the ep center-of-mass energy squared.

Fermion pair production in the DIS is sensitive to the gluon density in the proton. By using DIS $t\bar{t}$ production, one can study the top component of the structure function at the small x region [9-10]. In this domain, the power-law behavior of the gluon distribution function

$xf_g(x, Q^2) \propto x^{1-\Delta}$ measures the intercept of the BFKL trajectory $\Delta = \Delta_{\text{BFKL}}(t = 0)$. The standard parameterization of the gluon distribution function for $x \rightarrow 0$ is given by

$$xf_g(x, Q^2)|_{x \rightarrow 0} = A_g(Q^2)x^{-\Delta},$$

where A_g is Q^2 dependent and Δ is strictly positive. The gluon exponent at low values of x at $Q^2 = 1 \text{ GeV}^2$ has been obtained by MSTW08 NLO is $0.428_{-0.057}^{+0.066}$ [11]. The effective exponent for the gluon distribution at $Q^2 = 10 \text{ GeV}^2$ and $x = 10^{-4}$ obtained by NNPDF3.0, CT14, MMHT14, ABM12, and CJ15 had values of 0.20, 0.15, 0.29, 0.15, and 0.14, respectively. The value obtained by fixed coupling LLx BFKL gives $\Delta \simeq 0.5$, which is the so-called hard-Pomeron exponent. The gluon exponent is determined and applied to the deep inelastic lepton nucleon scattering at low values of x in Ref.[12]. Ref.[13] used a form inspired by the double asymptotic x, Q^2 scaling. The hard -Pomeron behavior of the photon -proton cross section based on a simple power-law behavior and double asymptotic scaling (DAS) at low x values for $10 < W < 10^4 \text{ GeV}$ (where W^2 is the invariant mass squared of the hadronic system in the final state) in the kinematic range of very high energy electron -proton/ion collider(VHEep) is shown in Ref.[14]. The authors in Ref.[15] presented a tensor-Pomeron model, where it was applied to low- x deep inelastic lepton-nucleon scattering and photoproduction processes. In this model, in addition to the soft tensor Pomeron, a hard tensor Pomeron and Reggeon exchange was included. In this case, the hard-Pomeron intercept was determined to be $0.3008_{(-84)}^{(+73)}$ with the latest HERA data for $x < 0.01$.

In the very small x domain, one studies QCD at a high gluon density where ep collider kinematics reaches a maximum of $Q^2 \simeq 1 \text{ TeV}^2$ and $x \simeq 10^{-5..-6}$ for LHeC and 10^{-7} for FCC-he. The ep center-of-mass (CM) energy at the LHeC and FCC-he ranges reaches up to $\sqrt{s} \simeq 1.3$ and 3.5 TeV , about 4 and 10 times the CM energy range of ep collisions at HERA, respectively.

In this paper, we consider the top quark pair production by the collinear generalized double asymptotic scaling approach [16] at the LHeC and FCC-he in the 5-flavor scheme (5FS) at the LO and NLO approximations in QCD [17]. The interest in a measurement of the top pair production, especially at low x , is related to the determination of the gluon distribution. The gluon distribution function is directly related to the proton structure function. Theoretical analysis of the parameterization of the proton structure function at low x , in the context of the fulfillment of the Froissart prescriptions, is suggested in Ref.[18]. The authors in Refs. [19,20] derived the longitudinal structure function based on this method. We focus on the parameterization of the top structure function for $Q^2 < m_t^2$ and study the collinear approach to the parameterization of the top structure function in

a typical region of the LHeC and FCC-he extended from the HERA kinematics. In Ref.[18], the authors fitted the HERA DIS data on F_2^p at low x in a wide range of the momentum transfer ($1 \text{ GeV}^2 < Q^2 < 10^5 \text{ GeV}^2$). We use these kinematics according to the ep collider CM energies at high inelasticity.

Figure 1 shows the area used for the transition from the HERA to the LHeC and FCC-he regions. The rectangle, in this figure, represents the kinematics used for the top structure function into the parameterization of the proton structure function. Indeed, correlated bounds on the kinematic region at different values of Q^2 are obtained from the parameterization of the proton structure function, confronted with the HERA data. The kinematic values are $(Q_1^2, Q_2^2, Q_3^2) = (100, 1000, 3000) \text{ GeV}^2$ for the LHeC and FCC-he.

The top quark mass is $172 \pm 0.5 \text{ GeV}$, which has been

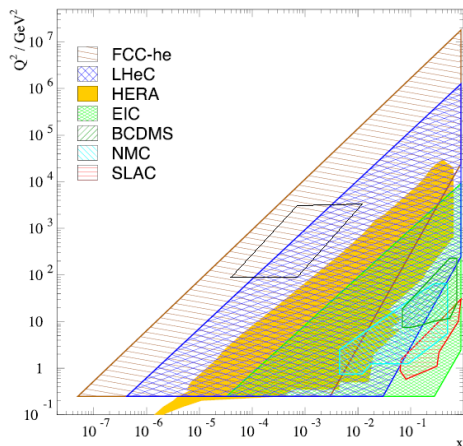


FIG. 1: The rectangle represents the coverage of the kinematic plane in deep inelastic lepton -proton scattering by the LHeC and FCC-he by extrapolating the HERA kinematic range to the top pair production. The kinematics used are $100 \text{ GeV}^2 \leq Q^2 \leq 3000 \text{ GeV}^2$ and $10^{-5} < x < 10^{-2}$. Inelasticity is defined according to the CM energies of ep colliders.

measured by ATLAS [21] and CMS [22] experiments. Here, $n_f = 5$ is normally taken for $\mu^2 < m_t^2$ at the top quark mass threshold, where μ^2 is the hard scale. Using $n_f = 5$ active flavors in the running of α_s is important for the precision phenomenology in the kinematics range $100 \text{ GeV}^2 \leq Q^2 \leq 3000 \text{ GeV}^2$.

The rest of our paper is organized as follows. In Sec. II, we present our theoretical framework of the top structure function into the parameterization of the proton structure function. In Sec. III, we show the numerical results for the top distribution and the implications to the measurement of the top cross section. Finally, in Sec. IV, we present our conclusions.

II. Theoretical framework

The top quark structure functions in DIS in the further ep colliders (i.e., LHeC and FCC-he) are obtained from the measurements of the inclusive heavy quark cross sections, which will be an important test of the QCD [1,2]. The reduced cross section of the top quark is defined in terms of the top structure functions by the following form:

$$\sigma_{\text{red}}^{t\bar{t}}(x, Q^2) = \frac{xQ^4}{2\pi\alpha_{EM}^2[(1+(1-y)^2)]} \frac{d^2\sigma^{t\bar{t}}}{dx dQ^2} = F_2^t(x, Q^2) - f(y)F_L^t(x, Q^2), \quad (7)$$

where $f(y) = \frac{y^2}{1+(1-y)^2}$. The electron -proton center of mass energies at the LHeC and FCC-he are proposed to be $\sqrt{s} \cong 1.3$ and 3.5 TeV , respectively. The ratio $R^t(x, Q^2) = F_L^t(x, Q^2)/F_2^t(x, Q^2)$ will extend in future circular colliders (i.e., LHeC and FCC-he). Indeed, these new colliders are the ideal place to resolve this ratio [1]. The photon-proton cross section for the top pair production, in the DIS, is related to the top structure function with the following form

$$\sigma_2^t(x, Q^2) = 4\pi^2\alpha_{EM}F_2^t(x, Q^2)/Q^2. \quad (8)$$

In the small x range, where the gluon contribution is dominant, the top structure functions in the collinear generalized DAS approach are given by [17]

$$F_k^t(x, Q^2) \simeq e^2 \sum_{n=0}^{\infty} \left(\frac{\alpha_s}{4\pi}\right)^{n+1} B_{k,g}^{(n)}(x, \xi) \otimes x f_g(x, \mu^2), \quad (9)$$

where $k = 2, L$ and $B_{k,g}$ are the collinear Wilson coefficient functions in the high energy regime. Their compact forms are defined in Ref.[17]. Here, n denotes the order in running coupling α_s and $\xi = \frac{m_t^2}{Q^2}$.

A NLO fit to the combined HERA data represents the power-like behavior of the gluon distribution. The low x asymptotic behavior of $f_g(x, \mu^2)$ is defined by the following form [16,24]

$$f_g(x, \mu^2)|_{x \rightarrow 0} \rightarrow \frac{1}{x^{1+\Delta}}. \quad (10)$$

We assume that this behavior holds for the gluon distribution function, in the LHeC and FCC-he energy range, that creates the top quark pair in the DIS processes [23]. According to the Dokshitzer-Gribov-Lipatov-Altarelli-Parisi (DGLAP) evolution equation, the singlet structure function at low x is defined by the gluon distribution as

$$\frac{\partial F_2^s(x, Q^2)}{\partial \ln Q^2} \simeq 2n_f \sum_{n=0}^{\infty} \left(\frac{\alpha_s}{2\pi}\right)^{n+1} P_{qg}^{(n)}(x) \otimes x f_g(x, \mu^2), \quad (11)$$

where $P_{qg}(x)$ is the quark-gluon splitting function. In Eqs. (9) and (11), the symbol \otimes is used for a

shorthand notation of the convolution formula, i.e., $f_1(x) \otimes f_2(x) \equiv \int_x^1 \frac{dy}{y} f_1(y) f_2(\frac{x}{y})$. After exploiting the low x asymptotic behavior of the gluon density (i.e., Eq.(10)), Eqs.(9) and (11) can be rewritten as

$$F_k^t(x, Q^2) \simeq M_{k,g}(x, \mu^2, \Delta) x f_g(x, \mu^2) \quad (12)$$

and

$$\frac{\partial F_2(x, Q^2)}{\partial \ln Q^2} \simeq N_{qg}(x, \mu^2, \Delta) x f_g(x, \mu^2), \quad (13)$$

where

$$\begin{aligned} N_{qg}(x, \mu^2, \Delta) &= \frac{5}{9} n_f \sum_{n=0} \left(\frac{\alpha_s}{2\pi}\right)^{n+1} \int_x^1 P_{qg}^{(n)}(y) y^{\Delta-1} dy \\ &= \frac{5}{9} n_f \int_x^1 \left[\frac{\alpha_s}{2\pi} P_{qg}^{(0)}(y) + \left(\frac{\alpha_s}{2\pi}\right)^2 P_{qg}^{(1)}(y) \right] y^{\Delta-1} dy \end{aligned} \quad (14)$$

and

$$\begin{aligned} M_{k,g}(x, \mu^2, \Delta) &= e_t^2 \sum_{n=0} \left(\frac{\alpha_s}{4\pi}\right)^{n+1} \int_x^{x_2} B_{k,g}^{(n)}(y, \xi) y^{\Delta-1} dy. \\ &= e_t^2 \int_x^{x_2} \left[\frac{\alpha_s}{4\pi} B_{k,g}^{(0)}(y, \xi) + \left(\frac{\alpha_s}{4\pi}\right)^2 B_{k,g}^{(1)}(y, \xi) \right] y^{\Delta-1} dy \end{aligned} \quad (15)$$

In the above equations (i.e., Eqs.(13-14) and (15)), $F_2 = \frac{5}{18} F_2^S$ ($F_2^S = x f_s$) and $x_2 = 1/(1+4\xi)$, respectively. Note that the superscript of the coefficients on the right-hand side represents the order in α_s . The standard representation for QCD couplings in the LO ($n=0$) and NLO ($n=1$) (within the $\overline{\text{MS}}$ -scheme) approximations reads

$$\begin{aligned} \alpha_s(t) &= \frac{4\pi}{\beta_0 t} & (\text{LO}), \\ \alpha_s(t) &= \frac{4\pi}{\beta_0 t} \left[1 - \frac{\beta_1 \ln \ln(t)}{\beta_0^2 t} \right] & (\text{NLO}), \end{aligned}$$

with β_0 and β_1 as the first two coefficients of the QCD β -function as

$$\beta_0 = \frac{1}{3}(11C_A - n_f), \quad \beta_1 = \frac{1}{3}(34C_A^2 - 2n_f(5C_A + 3C_F)),$$

where $C_F = \frac{N_c^2 - 1}{2N_c}$ and $C_A = N_c$ are the Casimir operators in the fundamental and adjoint representations of the $\text{SU}(N_c)$ color group, and $t = \ln \frac{Q^2}{\Lambda^2}$ where Λ is the QCD cut-off parameter.

The top structure functions, with the gluonic dominant, i.e., Eq.(12), are obtained in the generalized DAS approach by the following forms

$$F_k^t(x, Q^2)|_g = \frac{M_{k,g}(x, \mu^2, \Delta)}{N_{qg}(x, \mu^2, \Delta)} \frac{\partial F_2(x, Q^2)}{\partial \ln Q^2}, \quad k = 2, L \quad (16)$$

where they are directly dependent on the derivative of the proton structure function. In the LO approximation,

Eq.(16) is independent of the running coupling α_s and at the high-order approximations, it depends on the running coupling.

By generalizing Eq.(11) to the singlet density, the singlet DGLAP evolution equation is rewritten as

$$\begin{aligned} \frac{\partial F_2^s(x, Q^2)}{\partial \ln Q^2} &= \sum_{n=0} \left(\frac{\alpha_s}{2\pi}\right)^{n+1} \left[P_{qq}^{(n)}(x) \otimes x f_s(x, \mu^2) \right. \\ &\quad \left. + 2n_f P_{qg}^{(n)}(x) \otimes x f_g(x, \mu^2) \right]. \end{aligned} \quad (17)$$

The power-law behavior of the singlet distribution function is introduced by the following form [16,24]

$$f_s(x, \mu^2)|_{x \rightarrow 0} \rightarrow \frac{1}{x^{1+\Delta}}, \quad (18)$$

where the singlet and gluon exponents in Eqs.(10) and (18) are assumed to be equal at the NLO approximation¹. Assuming the Regge-like behavior for the gluon and singlet distributions (i.e., Eqs.(10) and (18)), we obtain the following equation for the Q^2 derivative of the structure function F_2 as

$$\begin{aligned} \frac{\partial F_2(x, Q^2)}{\partial \ln Q^2} &= T_{qq}(x, \mu^2, \Delta) F_2(x, \mu^2) \\ &\quad + N_{qg}(x, \mu^2, \Delta) x f_g(x, \mu^2), \end{aligned} \quad (19)$$

where

$$\begin{aligned} T_{qq}(x, \mu^2, \Delta) &= \sum_{n=0} \left(\frac{\alpha_s}{2\pi}\right)^{n+1} \int_x^1 P_{qq}^{(n)}(y) y^{\Delta-1} dy \\ &= \int_x^1 \left[\frac{\alpha_s}{2\pi} P_{qq}^{(0)}(y) + \left(\frac{\alpha_s}{2\pi}\right)^2 P_{qq}^{(1)}(y) \right] y^{\Delta-1} dy \end{aligned} \quad (20)$$

Therefore, the top structure functions, with gluon and singlet distributions, are obtained in the generalized DAS approach by the following forms:

$$\begin{aligned} F_k^t(x, Q^2)|_{s+g} &= \frac{M_{k,g}(x, \mu^2, \Delta)}{N_{qg}(x, \mu^2, \Delta)} \left[\frac{\partial F_2(x, Q^2)}{\partial \ln Q^2} \right. \\ &\quad \left. - T_{qq}(x, \mu^2, \Delta) F_2(x, Q^2) \right]. \quad k = 2, L \end{aligned} \quad (21)$$

With the explicit form of the basic expression laid above (i.e., Eq.(21)), we can proceed to extract the top quark structure functions $F_{2,L}^t$ from the parameterization of the proton structure function at the LO and NLO approximations.

The parameterization of the proton structure function has been found [18] at low values of Bjorken x from fit to all of the HERA DIS data. This function includes an

¹ The Regge- and non-Regge-like behavior assumptions for the gluon and singlet distributions are explained in Ref.[25]

asymptotic (high energy) part that satisfies a saturated Froissart-bound behavior, with a vector-dominance-like mass factor in the parameterization as

$$F_2^p(x, Q^2) = F_{2,v}^p(x, Q^2) + F_{2,\text{asympt}}^p(x, Q^2) \quad (22)$$

where $F_{2,v}^p$ is a valence term, and $F_{2,\text{asympt}}^p$ is an asymptotic term that is assumed to have the Froissart-bounded form and reads

$$F_{2,\text{asympt}}^p(x, Q^2) = D(Q^2)(1-x)^\nu \sum_{m=0}^2 A_m(Q^2)L^m, \quad (23)$$

where Eq.(23) is determined from the asymptotic part of the real γ^*p cross section by the following form:

$$\begin{aligned} \sigma_{\text{asympt}}^p &= \lambda \frac{4\pi^2 \alpha_{EM}}{M^2} \left[c_0 + a_0 \ln \left(\frac{\nu}{m} \frac{2m^2}{\mu^2} \right) \right. \\ &\quad \left. + b_0 \ln^2 \left(\frac{\nu}{m} \frac{2m^2}{\mu^2} \right) \right]. \end{aligned} \quad (24)$$

The effective parameters in Eqs.(23) and (24) are defined in Ref.[18]. This parameterization method, suggested by the authors in Ref.[18], provides reliable proton structure function $F_2(x, Q^2)$ with $x \leq 0.1$ in a wide range of the momentum transfer, $0.1 \text{ GeV}^2 < Q^2 \leq 5000 \text{ GeV}^2$.

A particular interest presenting the ratio of the top structure functions, due to Eqs.(16) or (21), is defined as

$$\begin{aligned} R^t(x, Q^2) &= \frac{F_L^t(x, Q^2)}{F_2^t(x, Q^2)} = \\ &= \frac{\sum_{n=0}^{\infty} \left(\frac{\alpha_s}{4\pi}\right)^{n+1} \int_x^{x_2} B_{L,g}^{(n)}(y, \xi) y^{\Delta-1} dy}{\sum_{n=0}^{\infty} \left(\frac{\alpha_s}{4\pi}\right)^{n+1} \int_x^{x_2} B_{2,g}^{(n)}(y, \xi) y^{\Delta-1} dy}. \end{aligned} \quad (25)$$

This is comparable to those in the generalized DAS approach (see [17]). Using the definition of the top structure function F_2^t in Eq.(21), the result for the $\gamma^* - p$ cross section due to Eq.(8) is obtained by the following form:

$$\begin{aligned} \sigma_2^t(x, Q^2) &= \frac{4\pi^2 \alpha_{em}}{Q^2} \frac{M_{2,g}(x, \mu^2, \Delta)}{N_{qg}(x, \mu^2, \Delta)} \left[\frac{\partial F_2(x, Q^2)}{\partial \ln Q^2} \right. \\ &\quad \left. - T_{qq}(x, \mu^2, \Delta) F_2(x, Q^2) \right]. \end{aligned} \quad (26)$$

Therefore, it is straightforward to evaluate the $\gamma^* - p$ cross section using the parameterization $F_2^p(x, Q^2)$ and its derivatives.

III. RESULTS

We study the top pair quark production in ep collisions at the LHeC and FCC-he CM energies in the collinear generalized DAS approach. Using the expression in Eq.(23) and extending the region of data to lower

x values, according to Fig.1 in Ref.[18], particular attention is paid to kinematics of low and ultra-low values of the Bjorken variable x , $10^{-5} < x < 10^{-2}$. The validity of this extension could be checked in the future at the proposed LHeC and FCC-he colliders. In further ep colliders, the center-of-mass energy increases. Therefore, with the decrease in the Bjorken variable x , it is possible to keep $sx = \frac{Q^2}{y}$ constant.

The strong coupling constant $\alpha_s(M_z^2) = 0.118$ and the running top quark mass $m_t = 172.5 \text{ GeV}$ are used throughout all the calculations. To estimate the scale uncertainties of our calculations, the standard variations in default renormalization and factorization scales, which were set to be equal to $\mu_R^2 = 4m_t^2 + Q^2$ and $\mu_F^2 = Q^2$, respectively, were introduced. The scale variations are calculated by varying the virtuality from $Q^2 = 100 \text{ GeV}^2$ to $Q^2 = 3000 \text{ GeV}^2$. Note that the exponent Δ for the power-like behavior $x^{-\Delta}$ of the collinear PDFs is considered to be $\simeq 0.29$ or $\simeq 0.50$ for the definition of the uncertainties in our calculations. The value of the exponent $\Delta \simeq 0.29$ [26] agrees with the independent fit to the DIS experimental data based on the hard Pomeron conjecture leading to the exponent value 0.30 ± 0.1 .

Our numerical results for the top structure function, the ratio $R^t(x, Q^2)$, and the top cross section are shown in Figs.2-4 at the renormalization scale μ_R^2 for $\Delta \simeq 0.29$, respectively, in the LO and NLO approximations. Results of calculations due to the CM energies and comparison between the LHeC and FCC-he are presented in these figures.

In Fig.2, we present the x -dependence of the top

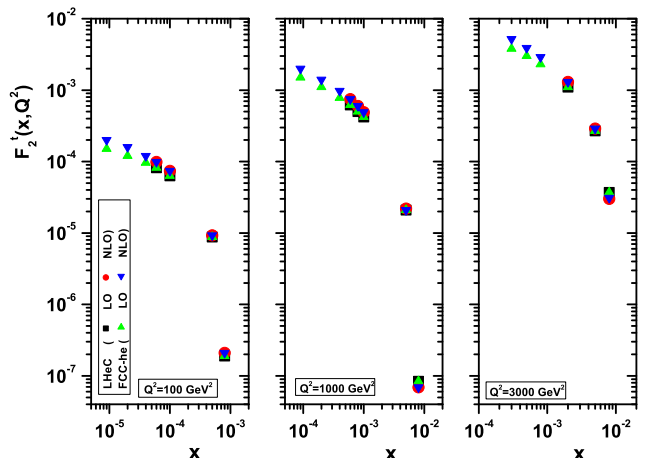


FIG. 2: The $\bar{t}t$ structure function prediction in the LHeC ($\sqrt{s} = 1.3 \text{ TeV}$) and FCC-he ($\sqrt{s} = 3.5 \text{ TeV}$) colliders in the LO and NLO approximations for $Q^2 = 100, 1000$ and 3000 GeV^2 at the renormalization scale $\mu_R^2 = 4m_t^2 + Q^2$ for $\Delta \simeq 0.29$, respectively.

structure function $F_2^t(x, Q^2)$ at $Q^2 = 100, 1000$, and 3000 GeV^2 in the LO and NLO approximations. The top structure functions increase as x decreases. With respect to the CM energies at the LHeC and FCC-he colliders, the results for the FCC-he are larger than the LHeC at very low values of x . Comparing the FCC-he and LHeC results, the FCC-he has a faster growth rate. In other places, the results are comparable. We observe that the top structure functions increase as Q^2 increases, and this is consistent with the pQCD.

In Fig.3, the x dependence of the ratio R^t is evaluated at the LO and NLO approximations with $\mu_R^2 = Q^2 + 4m_t^2$ for $\Delta \simeq 0.29$. These results lead to more or less flat (in-

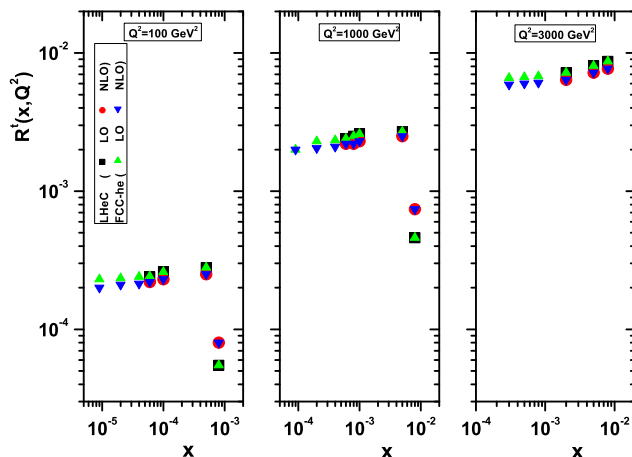


FIG. 3: R^t evaluated as functions of x in the LHeC ($\sqrt{s} = 1.3 \text{ TeV}$) and FCC-he ($\sqrt{s} = 3.5 \text{ TeV}$) colliders at the LO and NLO approximations with $\mu_R^2 = Q^2 + 4m_t^2$ for $Q^2 = 100, 1000$ and 3000 GeV^2 .

dependent on x) behavior of $R^t(x, Q^2)$ with $R^t \simeq 0.0002$ at $Q^2 = 100 \text{ GeV}^2$ and $R^t \simeq 0.006$ at $Q^2 = 3000 \text{ GeV}^2$ values. There is a tendency for the ratio $R^t(x, Q^2)$ to be almost independent of x in each bin of Q^2 for very low x and increasing with Q^2 increase for $Q^2 \ll m_t^2$, as it should be. The behavior of the ratio $R^t(x, Q^2)$ is in complete agreement with the usual statement about the property of k_T -factorization for $Q^2 < 5000 \text{ GeV}^2$, which grows faster when Q^2 increases.

Photon -proton cross section for the top pair production is related to the top structure function by Eq.(8). In figure 4, we show results for $\sigma_2^t(x, Q^2)$ as a function of x for different Q^2 below m_t^2 . Evolution of the $t\bar{t}$ cross sections as a function of x at the LO and NLO approximations in the LHeC ($\sqrt{s} = 1.3 \text{ TeV}$) and FCC-he ($\sqrt{s} = 3.5 \text{ TeV}$) colliders is shown in Fig.4. These values increase as x decreases. As a result, we predict that at very low x (i.e., at high inelasticity), the data will increase at the FCC-he than the LHeC.

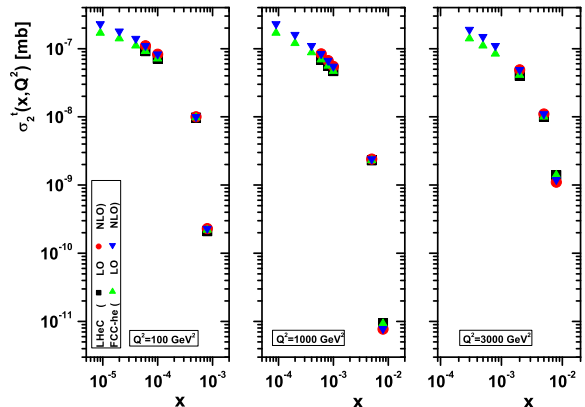


FIG. 4: Behavior of the $t\bar{t}$ cross section as function of x at the LO and NLO approximations in the LHeC ($\sqrt{s} = 1.3 \text{ TeV}$) and FCC-he ($\sqrt{s} = 3.5 \text{ TeV}$) colliders with $\mu_R^2 = Q^2 + 4m_t^2$ for $Q^2 = 100, 1000$ and 3000 GeV^2 .

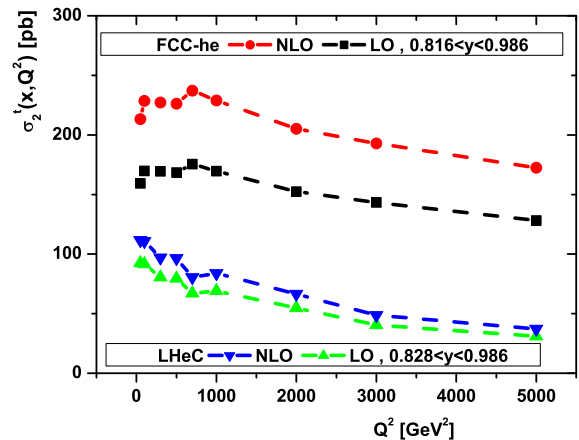


FIG. 5: γ^*p cross -sections σ_2^t as functions of Q^2 for fixed \sqrt{s} for $0.8 < y < 1$ at the LO and NLO approximations with $\mu_R^2 = Q^2 + 4m_t^2$ for $\Delta \simeq 0.29$.

In figure 5, we plot γ^*p cross sections for the LHeC and FCC-he CM energies as functions of Q^2 at high inelasticity. One can see that in both cases the cross -sections, for inelasticity $0.8 < y < 1$, decrease as Q^2 increases. The Q^2 dependence of σ_2^t in ep colliders is obtained at the LO and NLO approximations with $\mu_R^2 = Q^2 + 4m_t^2$ for $\Delta \simeq 0.29$ in this figure (i.e., Fig.5). It turns out that these values at the LO and NLO approximations with the renormalization scale numerically lead to

$$\begin{aligned} 30 \text{ pb} < \sigma_2^t(\text{LHeC}) < 130 \text{ pb}, \quad 0.828 \leq y \leq 0.986 \\ 130 \text{ pb} < \sigma_2^t(\text{FCC-he}) < 250 \text{ pb}, \quad 0.816 \leq y \leq 0.986 \end{aligned} \quad (27)$$

We observe that the difference between the LO and NLO results is small and the extracted top cross sections are comparable for the LHeC CM energy. This difference between the LO and NLO results is large for the FCC-he CM energy. We observe that the results for the top cross sections, for a fixed Q^2 , at the FCC-he are larger than the LHeC at the LO and NLO approximations. We observe that the discrepancy between two considered future colliders tends to be more clearly pronounced at the NLO approximation.

To estimate the uncertainties of our calculations, the standard variations in default scales (i.e., renormalization and factorization) and the behavior of the Δ -exponents are introduced. We present in Figs.6-8 the results for the top properties at the NLO approximation with the FCC-he CM energy for $Q^2 = 1000 \text{ GeV}^2$. The

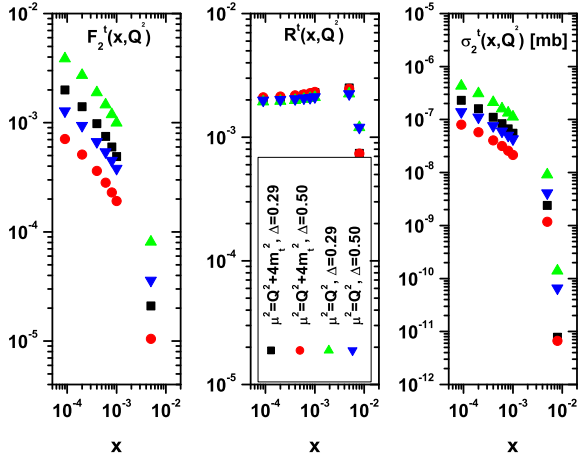


FIG. 6: x dependence of F_2^t , R^t and σ_2^t at $Q^2 = 1000 \text{ GeV}^2$ for the FCC-he CM energy at the NLO approximation for $0.8 < y < 1$. Plotted are $\mu^2 = Q^2 + 4m_t^2$ with $\Delta \simeq 0.29$ (black -squares), $\mu^2 = Q^2 + 4m_t^2$ with $\Delta \simeq 0.50$ (red -circles), $\mu^2 = Q^2$ with $\Delta \simeq 0.29$ (green -up triangles) and $\mu^2 = Q^2$ with $\Delta \simeq 0.50$ (blue -down triangles).

uncertainty range corresponds to the renormalization scale $\mu^2 = Q^2 + 4m_t^2$ with $\Delta \simeq 0.29$ and 0.50 , and the factorization scale $\mu^2 = Q^2$ with $\Delta \simeq 0.29$ and $\simeq 0.50$, respectively. In Fig.6, the difference between F_2^t and σ_2^t is clear when we compare these results with the different scales and exponents. One can see that the results obtained with the factorization scale $\mu^2 = Q^2$ with $\Delta \simeq 0.29$ are larger than others in a wide region of x . Our predictions for the ratio of structure functions are presented here, although they are fairly close.

Fig.7 shows the quantity σ_2^t as a function of Q^2 for the FCC-he CM energy at the NLO approximation with respect to the renormalization and factorization scales with $\Delta \simeq 0.29$ and $\simeq 0.50$, respectively. One can

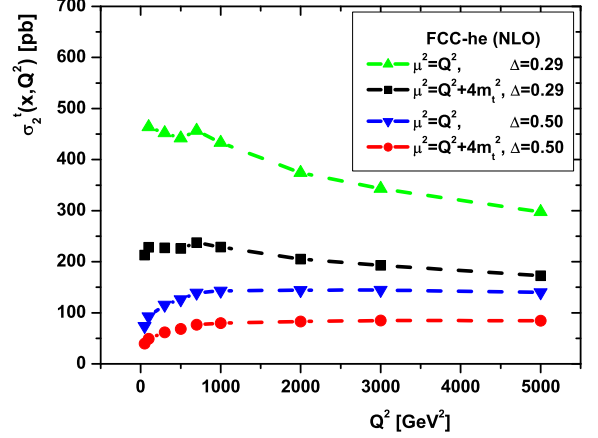


FIG. 7: Q^2 dependence of σ_2^t with the FCC-he CM energy at the NLO approximation for $0.8 < y < 1$. Plotted are $\mu^2 = Q^2 + 4m_t^2$ with $\Delta \simeq 0.29$ (black -squares) and $\Delta \simeq 0.50$ (red -circles), $\mu^2 = Q^2$ with $\Delta \simeq 0.29$ (green -up triangles), and $\Delta \simeq 0.50$ (blue -down triangles).

see that corrections due to the scales and exponents are sizable in a wide range of Q^2 . We see that, in this case, the factorization scale with $\Delta \simeq 0.29$ to σ_2^t is strongly different in comparison with the others.

Our numerical results due to the theoretical uncertain-

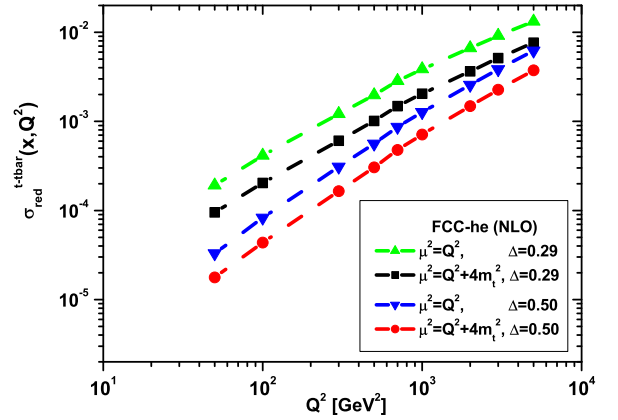


FIG. 8: The reduced top cross sections $\sigma_{\text{red}}^{t\bar{t}}$ as a function of Q^2 at the NLO approximation with the FCC-he CM energy for $0.8 < y < 1$ calculated at the scale $\mu^2 = Q^2 + 4m_t^2$ with $\Delta \simeq 0.29$ (black -squares) and $\Delta \simeq 0.50$ (red -circles), and at the scale $\mu^2 = Q^2$ with $\Delta \simeq 0.29$ (green -up triangles) and $\Delta \simeq 0.50$ (blue -down triangles).

ties for reduced cross section $\sigma_{\text{red}}^{t\bar{t}}$ are shown in Fig.8. In this figure (i.e., Fig.8), the Q^2 dependence of the

top reduced cross section is investigated at the NLO approximation due to the FCC-he CM energy. The top reduced cross sections increase as Q^2 increases. One can see again that the results obtained with the scale $\mu^2 = Q^2$ and $\Delta \simeq 0.29$ are larger than others in a wide region of x and Q^2 . It is clear that the discrepancy between two considered scale tends to be more clearly pronounced at small Q^2 . The uncertainties obtained for the top reduced cross section extend into the range $10^{-5} < \sigma_r^{tt} \leq 10^{-2}$ for $50 \leq Q^2 \leq 5000 \text{ GeV}^2$.

IV. CONCLUSIONS

In this paper, we present an overview of the top structure function in future ep colliders that relies on the Froissart-bounded parameterization of the proton structure function in the collinear generalized DAS approach. We focus our attention on the kinematic region of low x in an interval of the momentum transfer $Q^2 < m_i^2$. The top structure functions, the ratio of structure functions, and the top cross sections have been considered within the LO and next-to-leading order (NLO) approximations. The obtained explicit expressions for the selected topics are entirely determined by the effective parameters of the parameterization of the proton structure function. In principle, due to the largeness of the CM energies in the LHeC and FCC-he colliders, the x -dominated region expands toward the lower values while the Q^2/y remains constant, and we can use the HERA parameterization of the proton structure function that describes fairly well the available experimental data on the reduced cross sections.

The top cross sections extracted within the kinematic conditions that will correspond to that will be available at the LHeC and FCC-he colliders. It is found that, at relatively small $Q^2 < m_i^2$, both LO and NLO results reproduce the same and uniform behavior well. We have performed an analysis of the x -evolution of the extracted $F_2^t(x, Q^2)$ and $\sigma_2^t(x, Q^2)$. We observe that the results increase as x decreases. The ratio of top structure functions, as a function of x , is obtained for the LHeC and FCC-he CM energies at the LO and NLO approximations. The behavior is in fairly good agreement with the results [17] obtained in the framework of the k_t -factorization method for the charm and bottom pair production. Furthermore, the top structure functions can be used to predict the top part of the neutrino-nucleon cross -sections at ultra-high energy.

We obtained the uncertainties at high inelasticity on the top properties from the collinear generalized DAS approach in the kinematic range of the FCC-he collider at the NLO approximation. We studied the dependence of the top reduced cross section on the uncertainties

due to the scales and exponents. It will be interesting to compare these uncertainties with future results from measurements of these top reduced cross sections in the future. Carrying these results to improve the modeling of the top quark properties is crucial toward probing optimally the properties of this quark with the full data expected to be interesting in the LHeC first, then in the FCC-he. Also, these results may be important for future experiments at the Electron-Ion Collider (EIC) and Electron-Ion Collider in China (EiCC) [27] at low x .

ACKNOWLEDGMENTS

The author thanks Razi University for financial support of this project. The author also thanks the PLB referee for his/her suggestions that helped improve the manuscript.

REFERENCES

1. LHeC Collaboration and FCC-he Study Group, P. Agostini et al., J. Phys. G: Nucl. Part. Phys. **48**, 110501(2021).
2. LHeC Study Group, J.L.Abelleira Fernandez et al., J. Phys. G: Nucl. Part. Phys. **39**, 075001(2012).
3. M.Klein, arXiv [hep-ph]:1802.04317; M.Klein, Ann.Phys.**528**, 138 (2016); N.Arместо et al., Phys.Rev.D**100**, 074022 (2019).
4. S.J.Brodsky, arXiv [hep-ph]: 1106.5820; H.Sun, arXiv [hep-ph]: 1710.06260; H.Denizli et al., Phys. Rev. D **96**, 015024 (2017); M.Gao and J.Gao, Phys. Rev. D **104**, 053005 (2021).
5. Gerhard A. Schuler, Nucl.Phys.B **299**, 21 (1988).
6. U. Baur and J.J. van der Bij, Nucl.Phys.B **304**, 451 (1988).
7. M. Drees and K. Grassie, Z. Phys. C **28**, 451 (1985); M. Glück and E. Reya, Phys. Lett.B **83**, 98 (1979); L.M. Jones and H.W. Wyld, Phys. Rev. D **17**, 759 (1978).
8. N.Ya.Ivanov, Nucl.Phys.B **814**, 142 (2009).
9. G.R.Boroun; Phys.Lett.B **744**, 142 (2015); Phys.Lett.B **741**, 197 (2015); Chin.Phys.C **41**, 013104 (2017); arXiv [hep-ph]:2109.09583; B.Rezaei and G.R.Boroun, EPL **130**, 51002 (2020).
10. Y.Kitadono, Phys.Lett.B **702**, 135 (2011); Y.Yu et al., J.Phys.G **45**, 125003 (2018); L.Han, Yan-Ju Zhang and Yao-Bei Liu, Phys.Lett.B **771**, 106 (2017).
11. R.D.Ball et al., Eur.Phys.J.C**76**, 383(2016).
12. A.D.Martin, W.J.Stirling and R.G.Roberts, Phys.Rev.D**50**, 6734(1994).
13. R.D.Ball and S.Forte, Phys.Lett.B**335**, 77(1994); R.D.Ball and S.Forte, Phys.Lett.B**336**, 77(1994).
14. A.Caldwell and M.Wing, Eur.Phys.J.C **76**, 463(2016); A.Caldwell et al., arXiv[hep-

- ph]:1812.08110(2018).
15. D.Britzger et al., Phys. Rev. D **100**, 114007 (2019).
 16. A.Yu.Illarionov, B.A.Kniehl and A.V.Kotikov, Phys. Lett. B **663**, 66 (2008); A.Yu.Illarionov, and A.V.Kotikov, Phys. Atom. Nucl. **75**, 1234 (2012); A.V.Kotikov et al., Lect.Notes Phys. **647**, 386(2004); N.Ya. Ivanov, Nucl.Phys.B **814**, 142 (2009).
 17. A.V.Kotikov, A.V.Lipatov and P.Zhang, Phys.Rev.D **104**, 054042 (2021).
 18. M. M. Block, L. Durand and P. Ha, Phys. Rev.D **89**, 094027 (2014).
 19. L.P.Kaptari, A.V.Kotikov, N.Yu.Chernikova and Pengming Zhang, Phys.Rev.D **99**, 096019 (2019).
 20. G.R.Boroun and B.Rezaei, Phys.Rev.D **105**, 034002 (2022).
 21. M.Aaboud et al. [ATLAS Collaboration], Eur.Phys.J.C **79**, 290 (2019).
 22. V.Khachatryan et al. [CMS Collaboration], Phys. Rev. D **93**,072004 (2016).
 23. Olga B.Bylund, arXiv [hep-ex]:2103.14772; P.Ferreira da Silva, arXiv [hep-ph]:1605.05343.
 24. J.R.Cudell and G.Soyez, Phys.Lett.B **516**, 77 (2001); A.Donnachie and P.V.Landshoff, Phys.Lett.B **533**, 277 (2002); Phys.Lett.B **595**, 393 (2004).
 25. A.V.Kotikov and G.Parente, Phys.Lett.B **379**, 195 (1996).
 26. D.Schildknecht, Phys.Rev.D **104**, 014009 (2021); G.R.Boroun, M.Kuroda and D.Schildknecht, arXiv [hep-ph]:2206.05672.
 27. A. Accardi et al., Eur. Phys. J. A **52**, 268 (2016); D. P. Anderle et al., Frontiers of Physics **16**, 64701 (2021).